

# Supporting Information

## The first small molecule inhibitors targeting the RNA binding protein IGF2BP2/IMP2 for cancer therapy

Charlotte Dahlem<sup>a,#</sup>, Ali Abuhaliema<sup>a,#</sup>, Sonja M. Kessler<sup>a,b,#</sup>, Tarek Kröhler<sup>a</sup>, Ben G. E. Zoller<sup>c</sup>, Shilpee Chanda<sup>a</sup>, Yingwen Wu<sup>c</sup>, Simon Both<sup>a</sup>, Fabian Müller<sup>d</sup>, Konstantin Lepikhov<sup>e</sup>, Susanne H. Kirsch<sup>f</sup>, Stephan Laggai<sup>a</sup>, Rolf Müller<sup>f,g</sup>, Martin Empting<sup>c,g</sup>, Alexandra K. Kiemer<sup>a,\*</sup>

<sup>a</sup> Department of Pharmacy, Pharmaceutical Biology, Saarland University, Saarbrücken, 66123, Germany

<sup>b</sup> Institute of Pharmacy, Experimental Pharmacology for Natural Sciences, Martin Luther University Halle-Wittenberg, Halle, 06108, Germany

<sup>c</sup> Department of Drug Design and Optimization, Helmholtz Institute for Pharmaceutical Research Saarland (HIPS), Helmholtz Centre for Infection Research (HZI), Saarland University, Saarbrücken, 66123, Germany

<sup>d</sup> Center for Bioinformatics, Saarland University, Saarbrücken, 66123, Germany

<sup>e</sup> Department of Genetics, Saarland University, 66123 Saarbrücken, 66123, Germany

<sup>f</sup> Department of Microbial Natural Products, Helmholtz Institute for Pharmaceutical Research Saarland (HIPS), Helmholtz Centre for Infection Research, Saarland University Campus, 66123 Saarbrücken, Germany

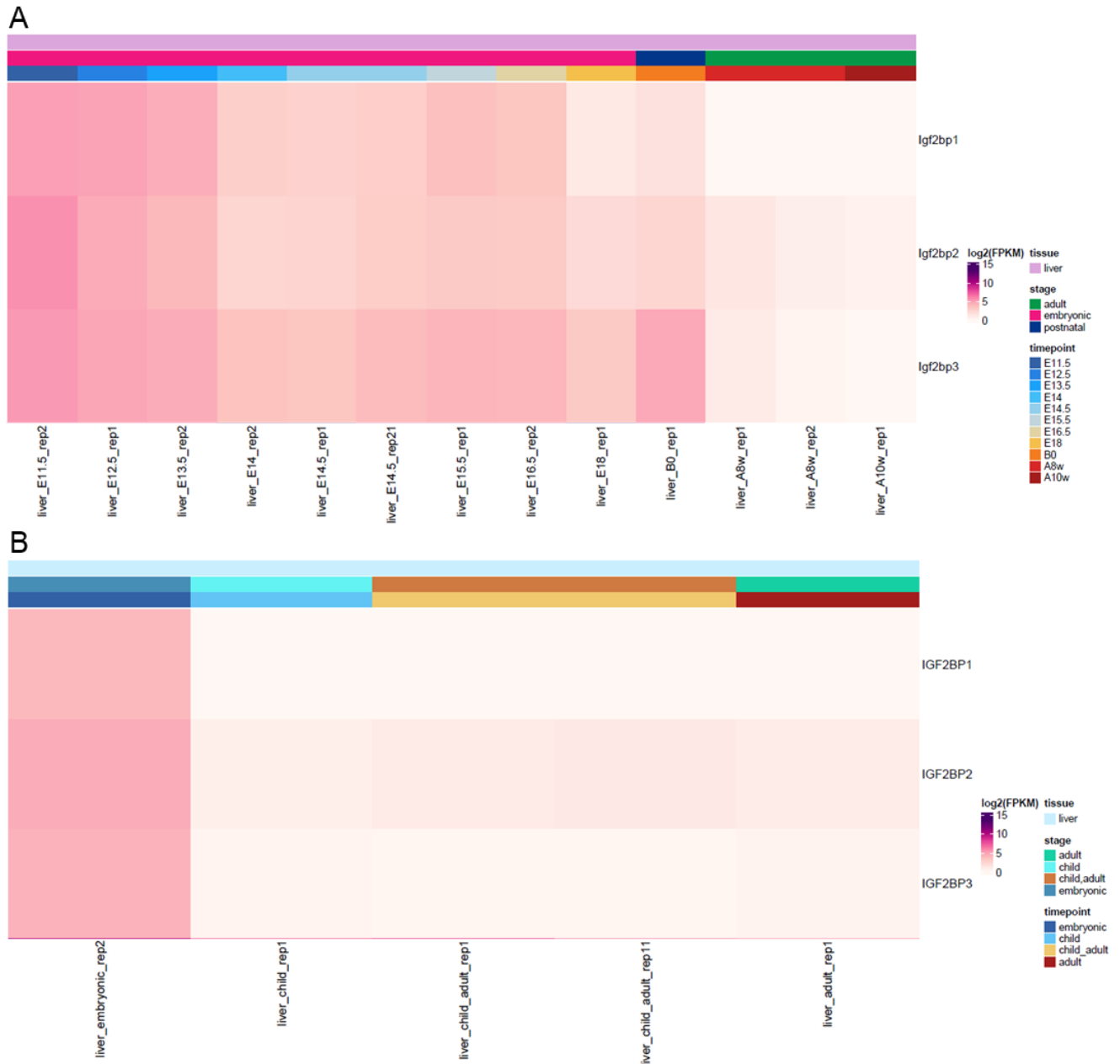
<sup>g</sup> Department of Pharmacy, Saarland University, Saarbrücken, 66123, Germany

<sup>#</sup> equal contribution

<sup>\*</sup> corresponding author

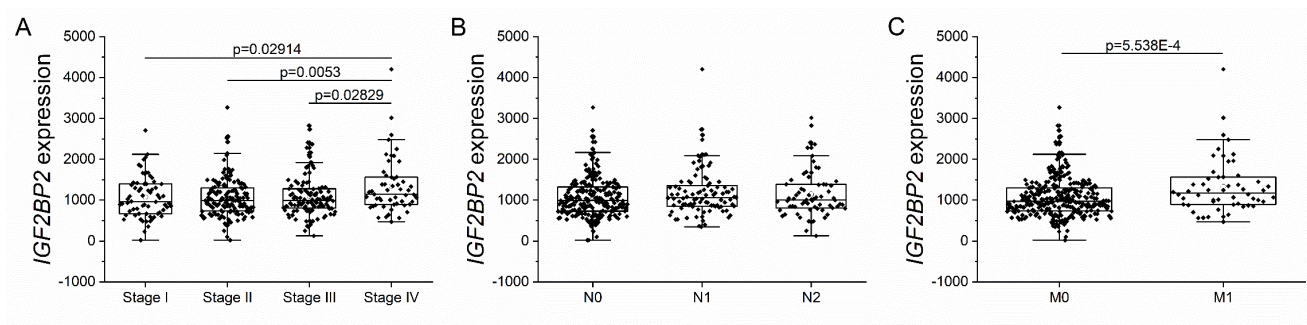
Alexandra K. Kiemer  
Saarland University  
Department of Pharmacy  
Pharmaceutical Biology  
Campus C2 3  
D-66123 Saarbrücken, Germany  
Fax: +49 681 3021 57302  
pharm.bio.kiemer@mx.uni-saarland.de

## Supplementary Figures



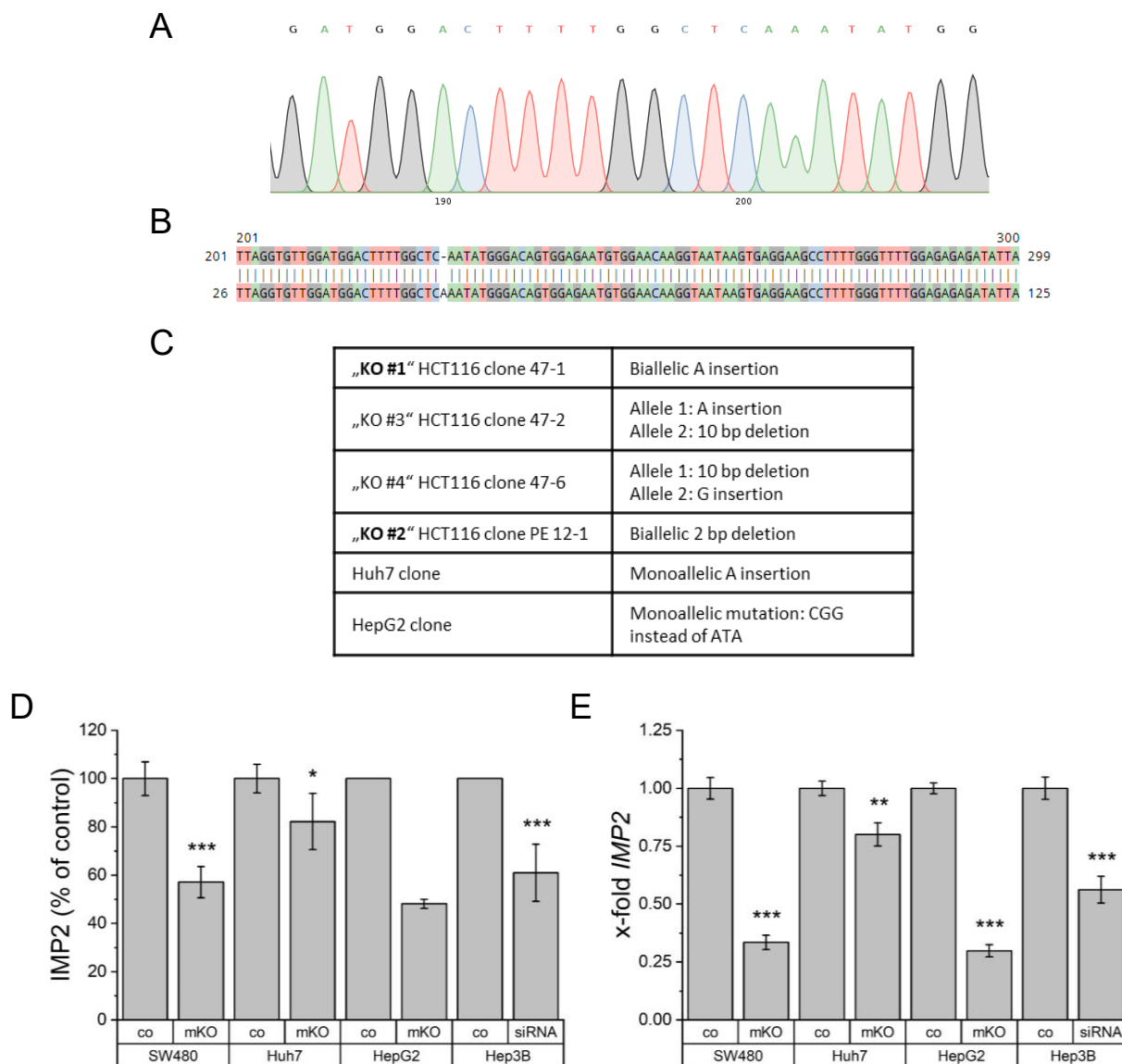
**Supplementary Figure S1. Comparison of *IGF2BP2* expression with *IGF2BP1* and *IGF2BP3* in murine and human embryonic and adult livers**

Gene expression levels (log<sub>2</sub> FPKM) for IGF2BPs 1-3 in (A) mouse liver and (B) human liver in different developmental stages. Data originated from a mouse developmental atlas and the ENCODE project.



### Supplementary Figure S2. *IGF2BP2* expression of COAD patients

Analyses of the *IGF2BP2* expression in the COAD dataset tumors characterized by (A) AJCC neoplasm disease stage and (B, C) pathology T/N/M stage.



### Supplementary Figure S3. Sanger sequencing of IMP2 CRISPR clones

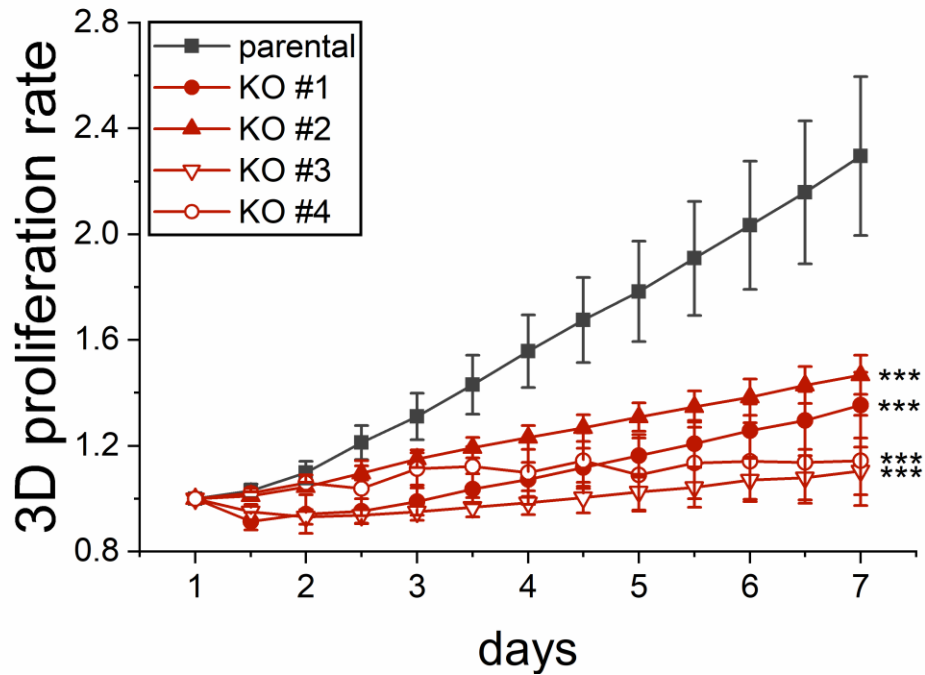
(A) Representative Sanger sequencing result of the IMP2 CRISPR HCT116 clone 47-1 that was used for target validation and compound testing (e.g., Figure 1 and Figure 5).

(B) Sequence alignment of IMP2 CRISPR HCT116 clone 47-1, demonstrating a bi-allelic A insertion.

(C) Table summarizing the editing of clones used in this study. HCT116 clone “KO #2” was generated using prime editing.

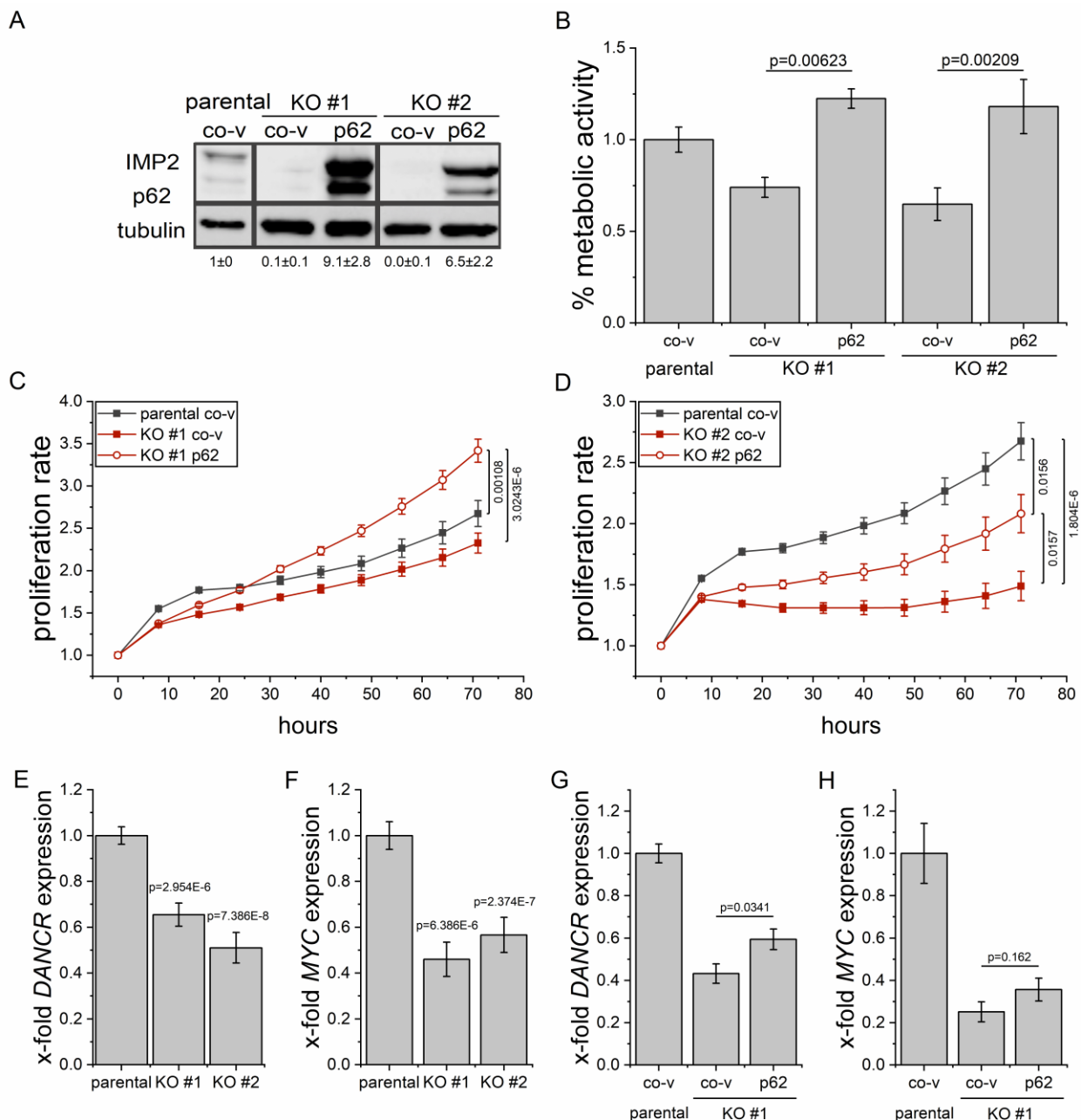
(D) Quantification of IMP2 protein levels in partial IMP2 knockdown cells compared to parental cells. Data are represented as means  $\pm$  SEM, n=2-6.

(E) Quantification of *IMP2* gene levels in partial IMP2 knockdown cells compared to parental cells. Data are represented as means  $\pm$  SEM, n=3.



**Supplementary Figure S4. 3D growth comparison of HCT116 knockout clones**

The spheroid growth of different HCT116 IMP2 knockout clones showing different gene edits (see Supplementary Figure S2) was monitored by automated live-cell microscopy, starting after spheroid formation for 24 h. Spheroid area was analyzed using the IncuCyte® S3 system and was normalized to 1-day old spheroids. Data are represented as means  $\pm$  SEM, n=3 (quadruplicates). Statistical analysis was performed for the last acquired time point (7 days). Asterisks represent values for the comparisons between the growth of parental and respective knockout cells. p values comparing the growth of different clones were  $> 0.05$ .



### Supplementary Figure S5. Target specificity of IMP2 knockout in HCT116 cells

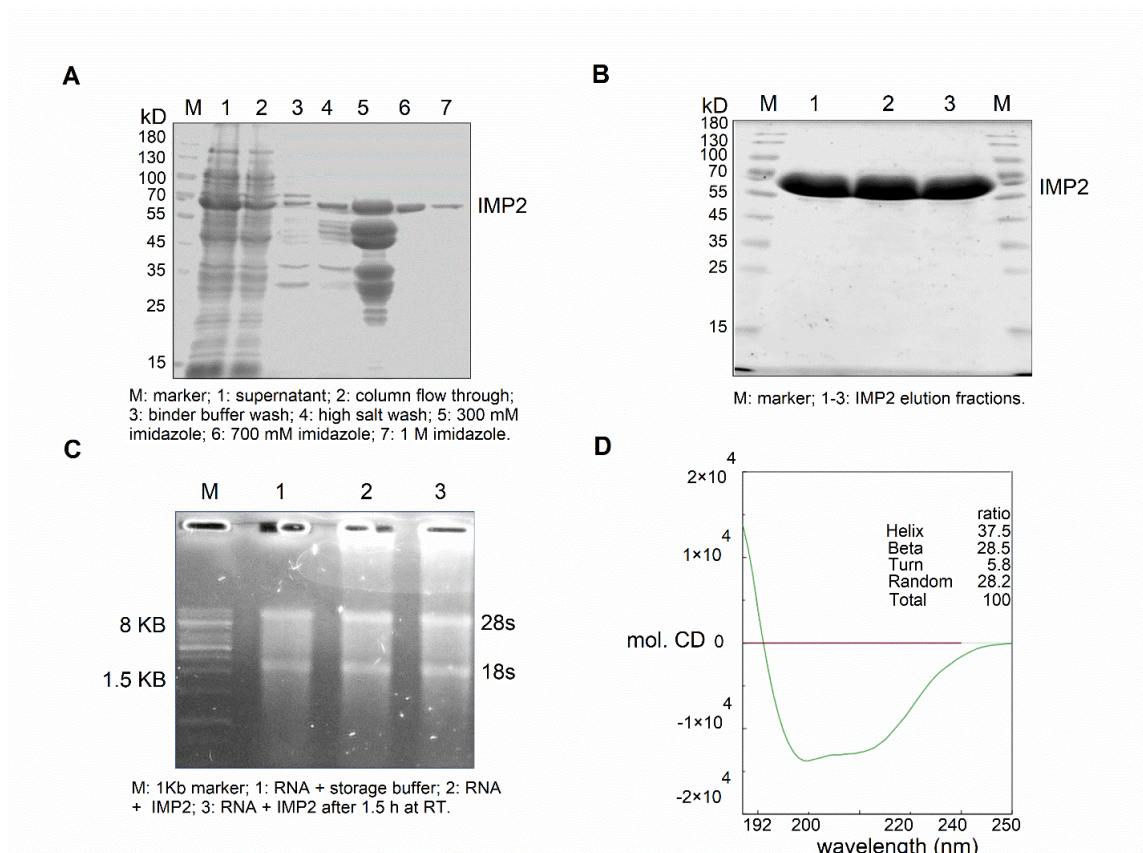
(A-D) HCT116 parental and IMP2 knockout HCT116 cells (CRISPR/Cas9 clone KO #1, prime editing clone KO #2) were transfected with p62/IMP2 or control vector (co-v).

(A) Transfection efficiency and p62/IMP2 overexpression was controlled by Western blot 3 days post transfection.

(B) Metabolic activity was measured *via* MTT assay 3 days post transfection.

(C, D) Cell confluency was monitored using the IncuCyte® S3 system over 3 days. Confluency was normalized to the time point of transfection (0 h). Data are represented as means ± SEM, n=2 (quadruplicates).

(E, F) *DANCR*, and *MYC* gene expression was determined in HCT116 IMP2 knockout clones and (G, H) p62/IMP2 overexpressing parental and knockout cells by qPCR. Values were normalized to the housekeeping gene *RNA18S*, n=3 (triplicates). Data are represented as means ± SEM.



### Supplementary Figure S6. IMP2 isolation and characterization

Histidine-tagged IMP2 was overexpressed in *E. coli* and isolated *via* affinity chromatography using a HisTrap HP Nickel–Sepharese column. Protein was eluted in an imidazole buffer with increasing imidazole concentrations.

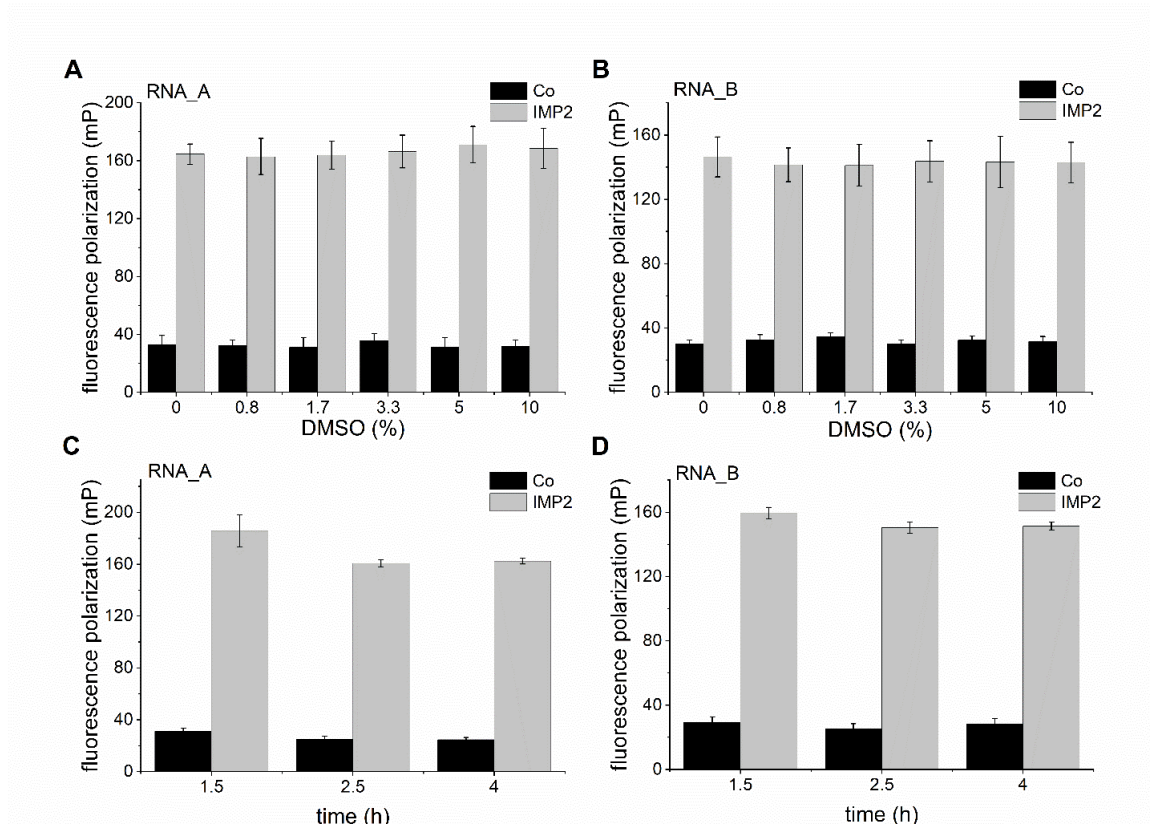
(A) Fractions were collected and run on an SDS-PAGE (lanes 5-7). A 10-180 kD protein ladder marker (M), the unpurified cell lysate (1), the column flow-through (2), and washing buffers (3-4) were also run on the gel. The gel was stained with Coomassie blue and revealed the pure IMP2 protein in the 300 mM and 700 mM imidazole fractions (lanes 6 and 7). IMP2 containing fractions were combined and concentrated.

(B) The identity of the 67 kDa protein IMP2 was confirmed by Western blot analysis.

(C) The absence of RNase activity was confirmed *via* RNA integrity measurement of MCF7 RNA in the presence of eluted protein, as visualized on an agarose gel. M: 1 kb marker, 1: RNA incubated with storage buffer for 1.5 h as a control, 2: RNA incubated with IMP2 for 1.5 h on ice, 3: RNA incubated with IMP2 for 1.5 h at room temperature (RT).

(D) Circular dichroism (CD) spectroscopy was used to verify the correct protein folding of the purified protein.



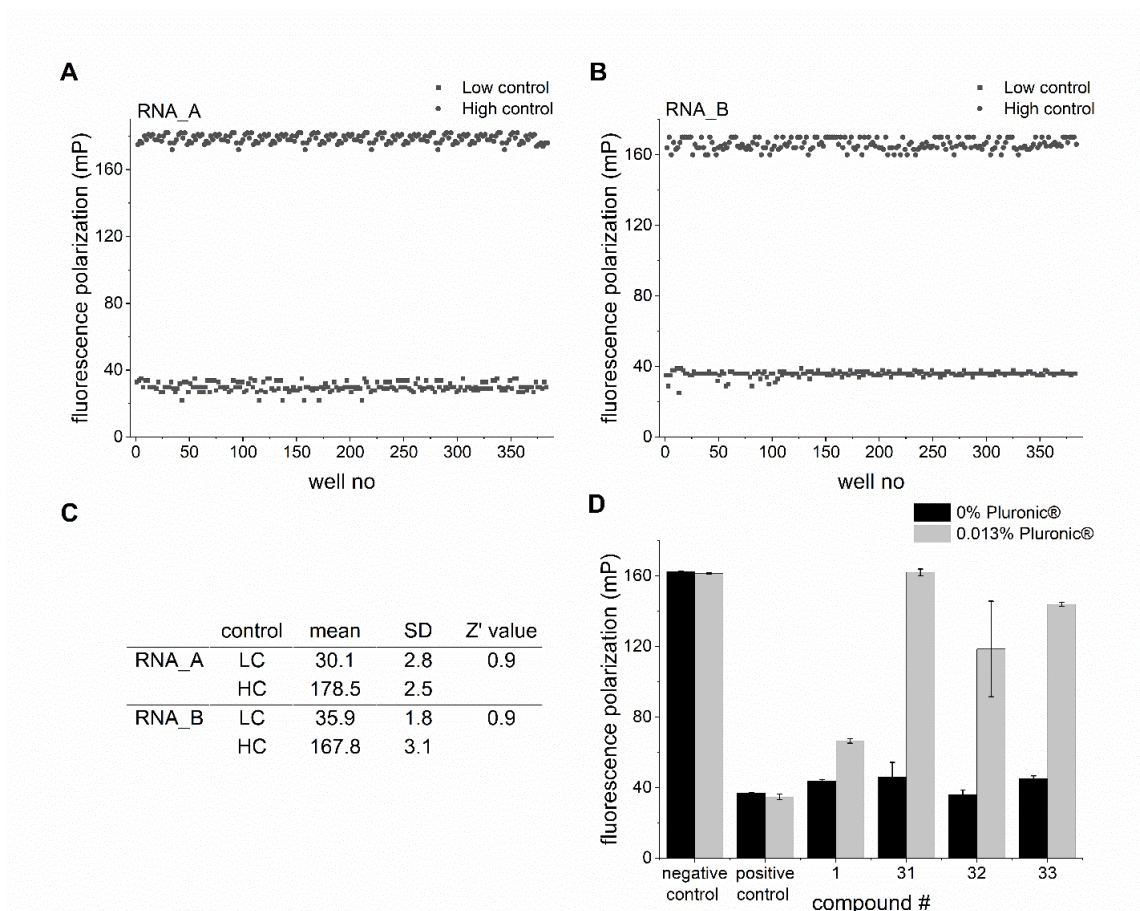


### Supplementary Figure S7. Fluorescence polarization assay development and validation

(A, B) The DMSO tolerance of the FP assay was determined by using 1 nM of either the (A) RNA\_A or the (B) RNA\_B probe, IMP2 (120 nM for RNA\_A and 160 nM for RNA\_B), and varying concentrations of DMSO v/v. Unlabeled RNA was used as a control.

(C, D) The stability of the protein-RNA complex was assessed for 5% DMSO at different time points. Data are represented as means  $\pm$  SD, n=2 (triplicates).



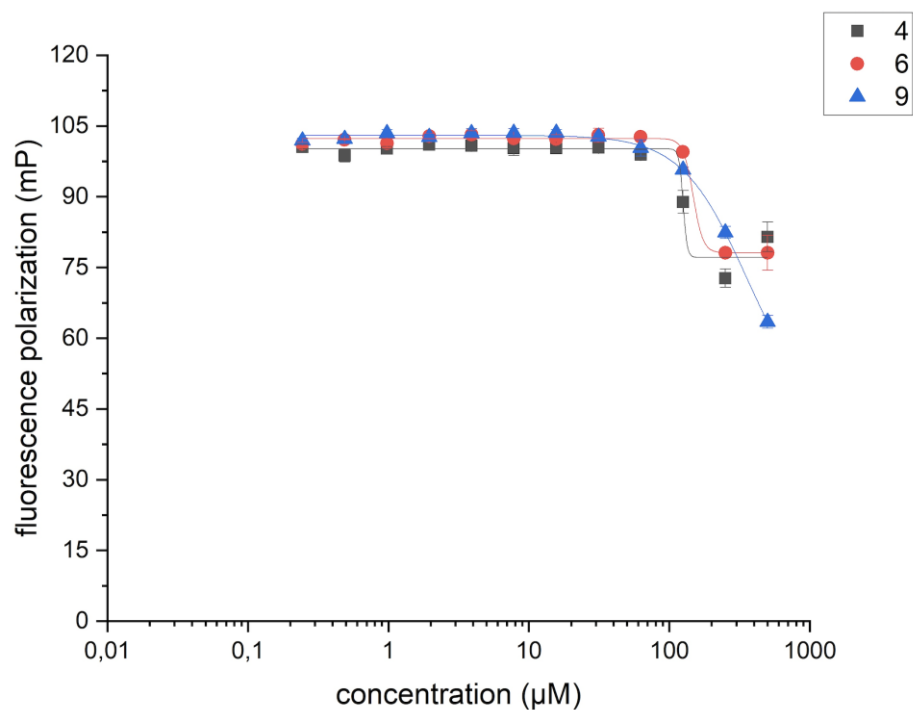


### Supplementary Figure S8. The robustness of the FP assay

(A, B) To determine the robustness of the FP assay, 192 samples of low controls (LC), containing 1 nM (A) RNA\_A or (B) RNA\_B without IMP2, and 192 samples of high controls (HC) containing additionally 120 nM and 160 nM IMP2 for RNA\_A and RNA\_B, respectively, were assessed at 5% DMSO in the FP assay after 1.5 h incubation.

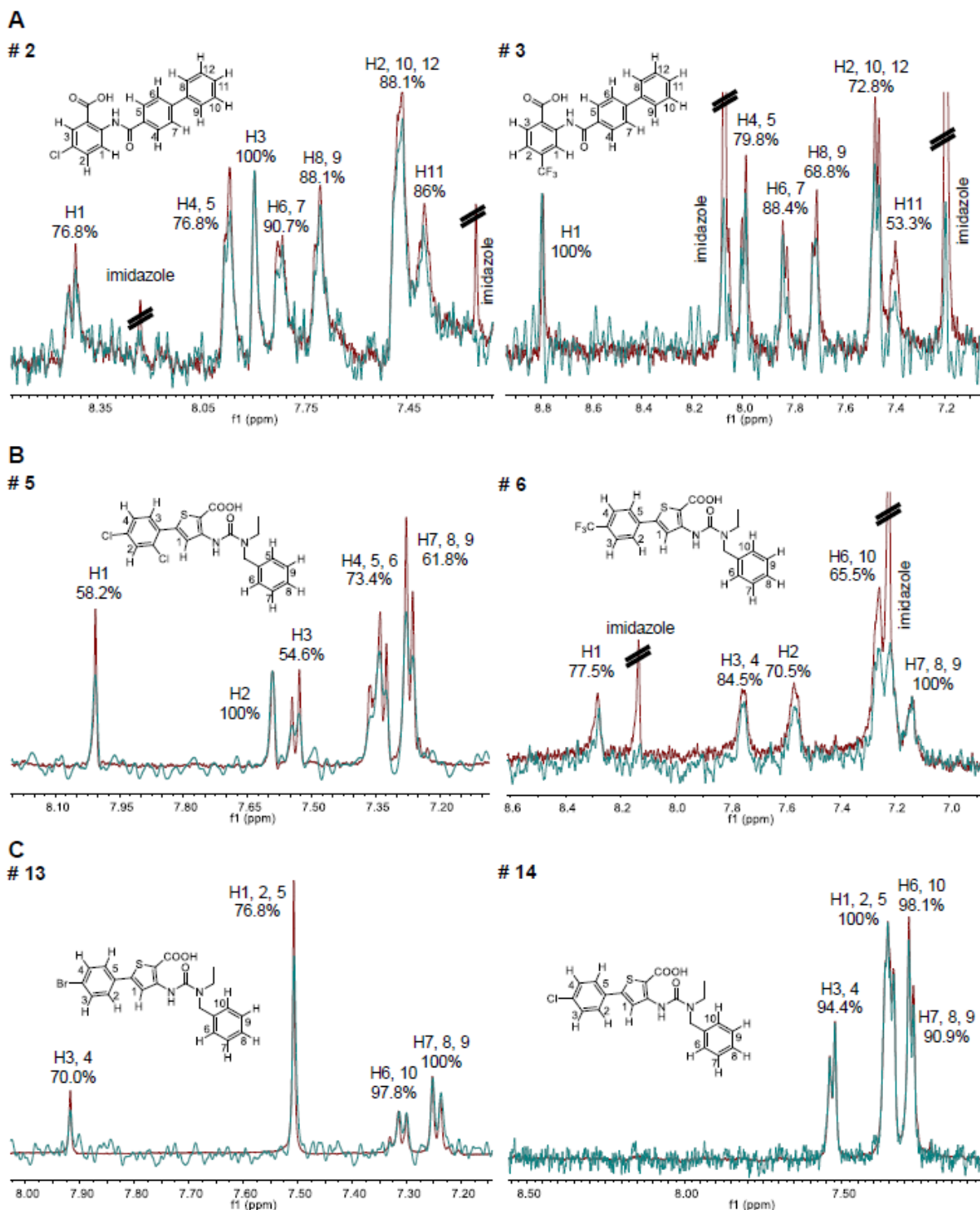
(C) Z'-factors were calculated based on the obtained data.

(D) To minimize unspecific aggregation and, therefore, false-positive results, 0.013% Pluronic® were added to FP buffer. The inhibitory effect of compounds **31** – **33** was lost after addition of Pluronic®, but not for compound **1**. Data are represented as means  $\pm$  SD, n=1 (duplicates).



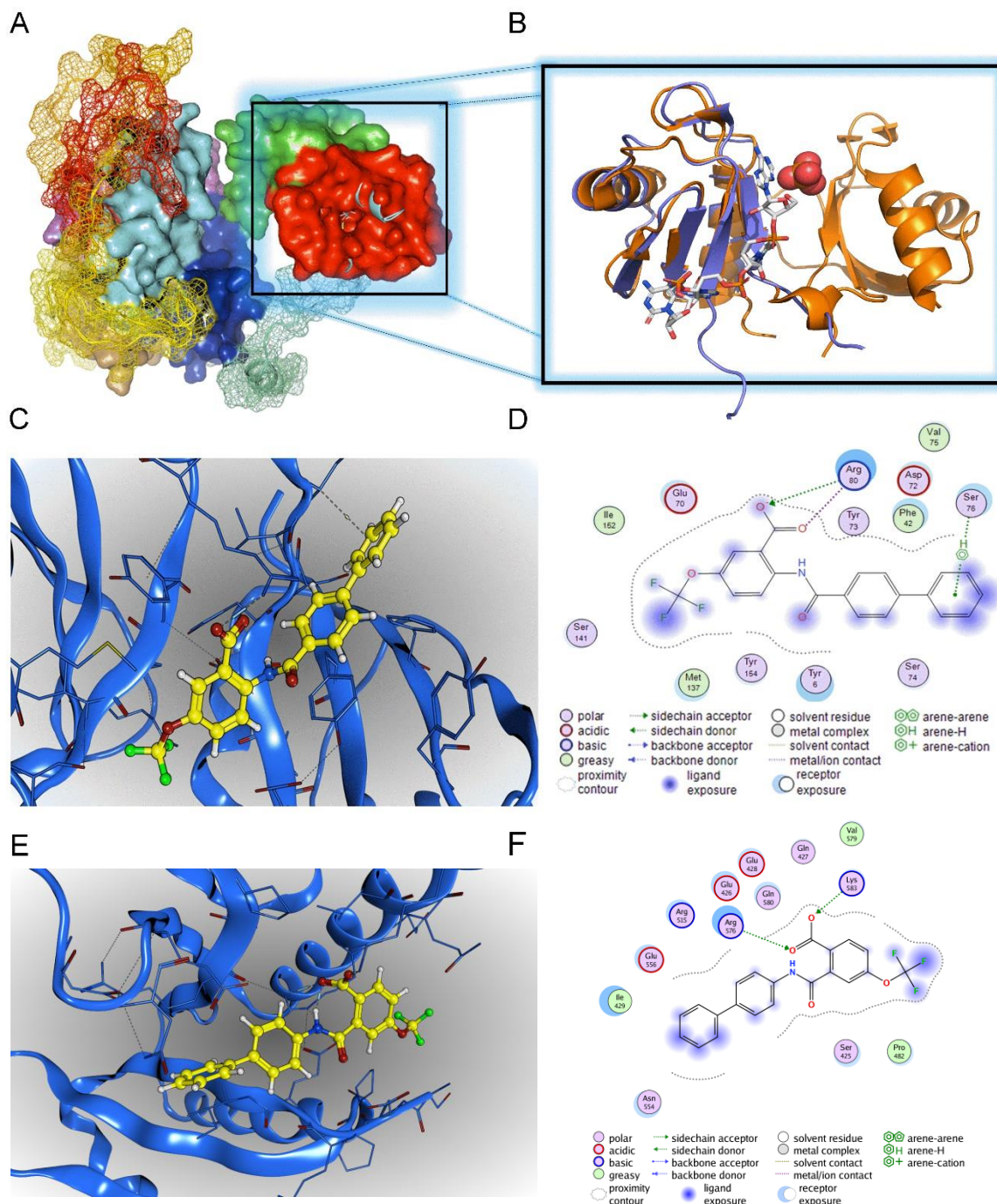
#### Supplementary Figure S9. Hit compounds tested against the RBP CsrA

Competition binding assays were performed by FP assay using CsrA from *Y. pseudotuberculosis* to test the specificity of IMP2:compound interactions. Hit compounds **4**, **6** and **9** were used in concentrations up to 500 μM to compete with the fluorescence labelled target RNA (15 nM) for CsrA (400 nM) binding.



**Supplementary Figure S10. STD-NMR analysis**

STD-NMR experiments were performed at fixed concentrations of 2.5-5  $\mu$ M IMP2 and either 250  $\mu$ M for compounds **2** and **3** or 500  $\mu$ M for compounds **5-6** and **13-14** based on the solubility limit in 10% DMSO  $D_6$  (molar ratio of protein to ligand was 1:100). Compounds **2** and **3** represent class A hit compounds (A), compounds **5** and **6** class B compounds (B), and compounds **13** and **14**, selective RNA<sub>A</sub> inhibitors (C). The reference spectrum without protein is shown in red, and the STD difference spectrum of the IMP2/compound complexes is shown in green. Overlaid STD off-resonance and STD effect spectra were normalized to the signal of the highest proton signal.



**Supplementary Figure S11. Molecular docking analysis of IMP complex**

(A) IMP2 structure prediction based on IMP2 homology modeling.

(B) Overlay of IMP2 RRM1 (blue), and IMP3 RRM12 (orange) crystals show 3D structure similarity.

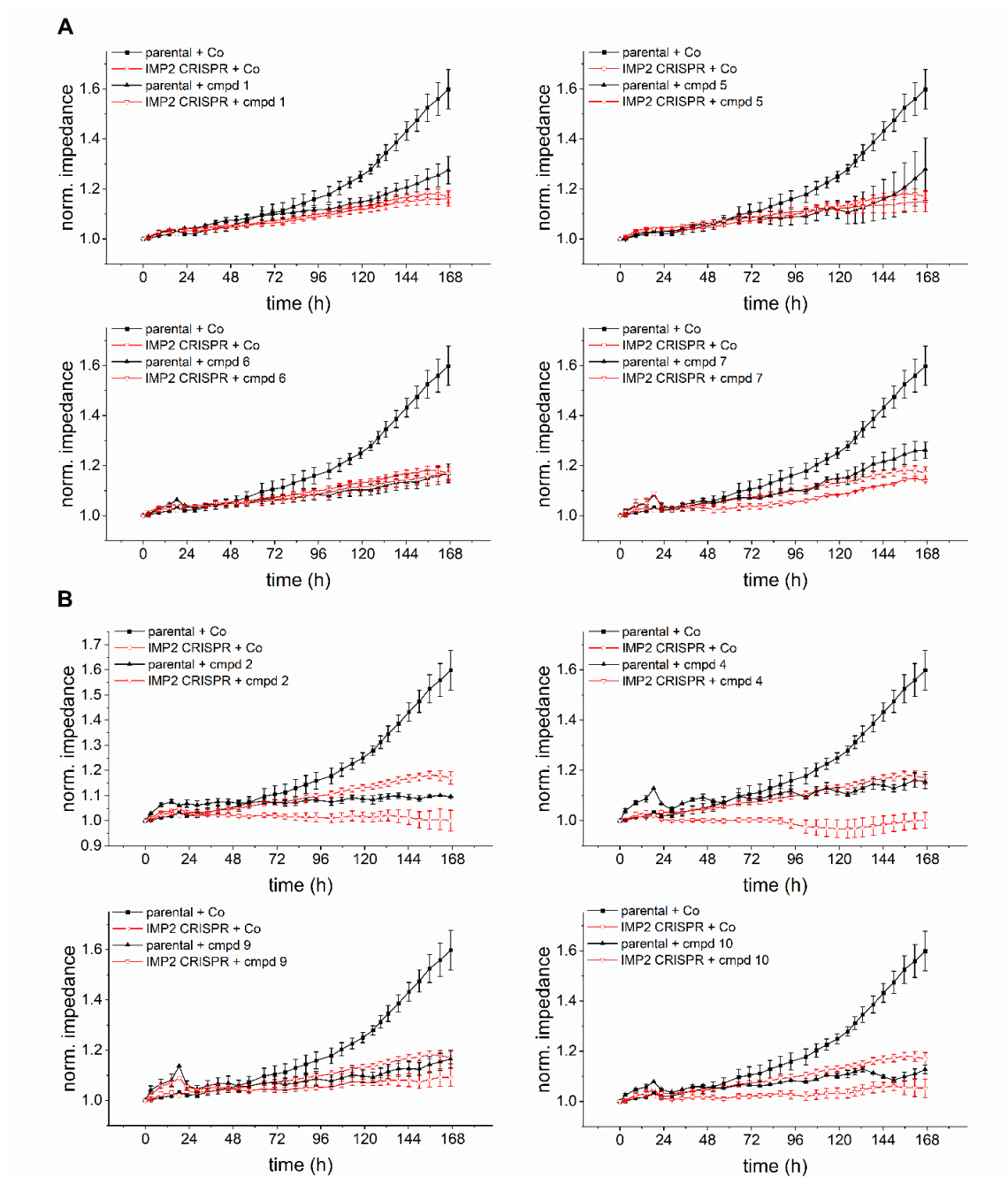
(C) 3D depiction of the docking-derived binding hypothesis for hit compound **4**. RNA binding sites on the IMP2 RRM1 homology model were identified based on IMP3 RRM12-binding RNA coordinates and used as the docking site.

(D) Ligand interaction scheme for the docking pose of compound **4** in complex with IMP2 RRM1.

(E) 3D depiction of the docking-derived binding hypothesis for hit compound **4** to the IMP2 KH34 domain. RNA binding sites on the IMP2 KH34 domain are reported in the literature and were used as docking site (Biswas et al., 2019).

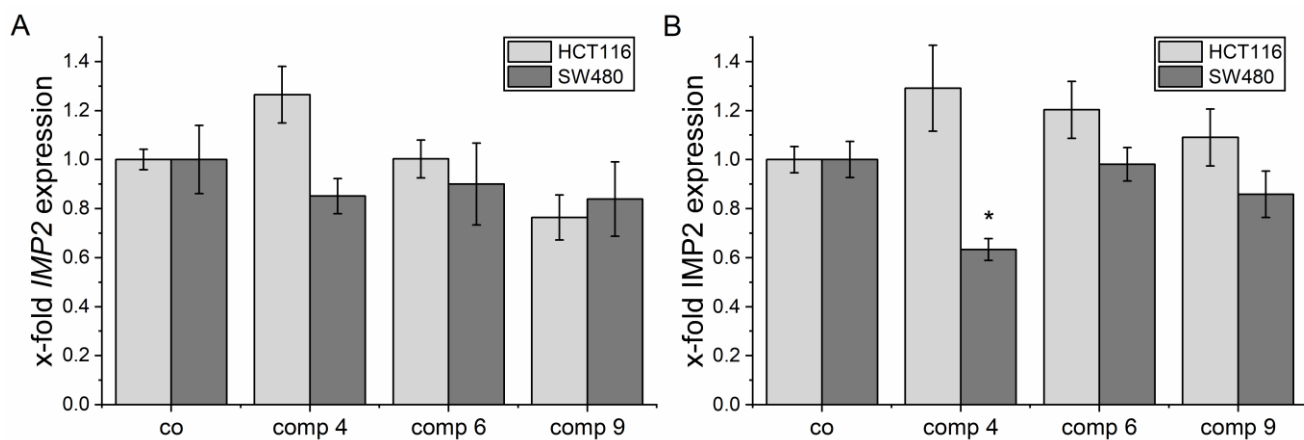
(F) Ligand interaction scheme for the docking pose of compound **4** in complex with the IMP2 KH34 domain.





**Supplementary Figure S12. Action of hit compounds in the absence of the target on cell impedance changes**

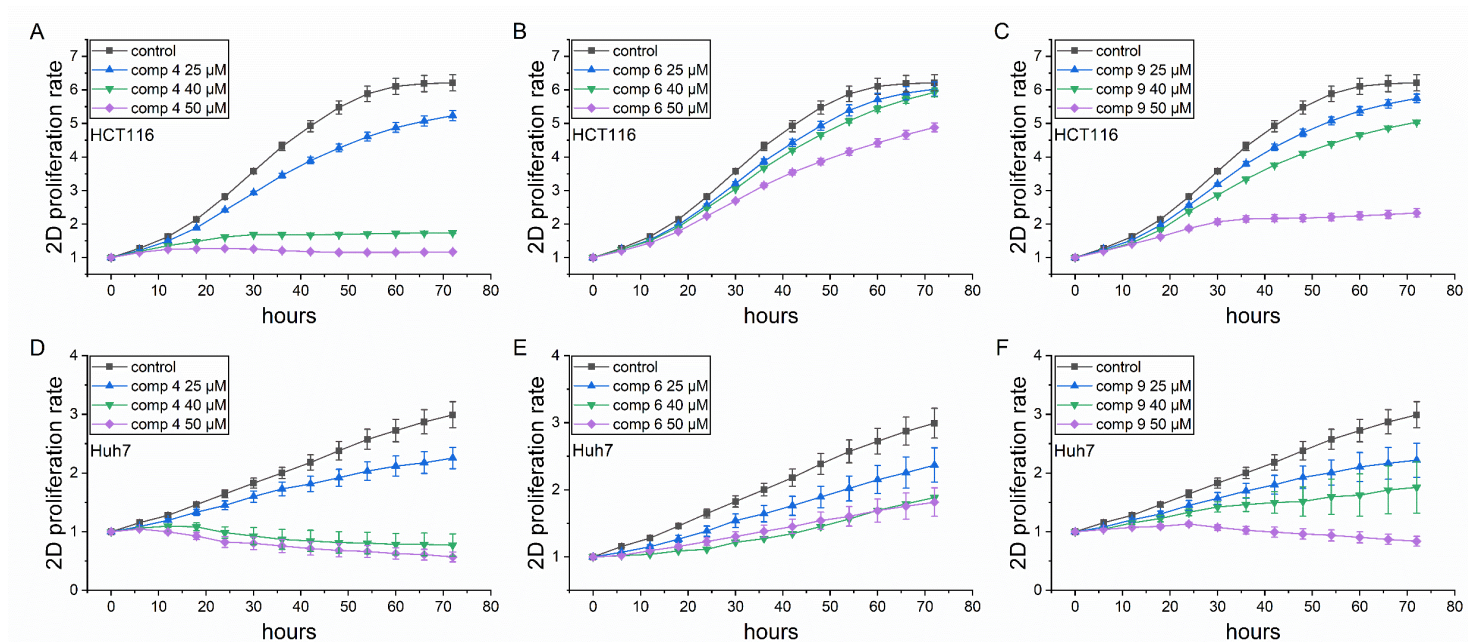
Cell impedance was assessed as readout parameter for cell density and adhesion. HCT116 parental and IMP2 CRISPR/Cas9 knockout cells were seeded in equal numbers and treated with 25  $\mu$ M of the respective compound or DMSO solvent control (co). Hit compounds demonstrated effective anti-proliferative effects in HCT116 parental cells but (A) no or (B) lower effects in IMP2 CRISPR cells. Data are represented as means  $\pm$  SEM, n=2 (triplicates).



**Supplementary Figure S13. Expression of IMP2 upon compound treatment**

(A) Quantification of *IMP2* gene levels of HCT116 and SW480 cells, treated with compound **4** (40  $\mu$ M), **6** (50  $\mu$ M), or **9** (50  $\mu$ M) for 24 h. Data are normalized to *RNA18S* and are represented as means  $\pm$  SEM, n=3.

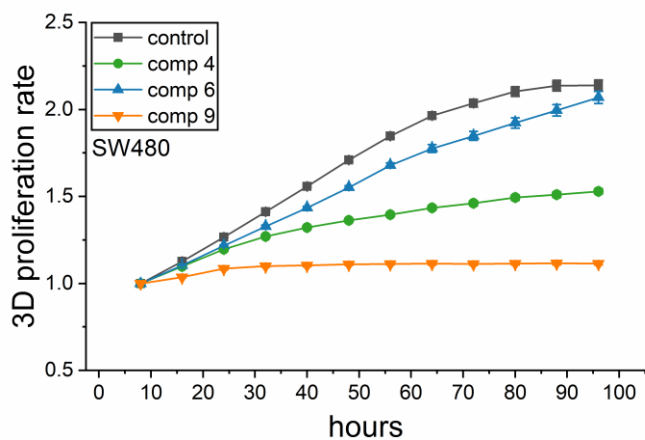
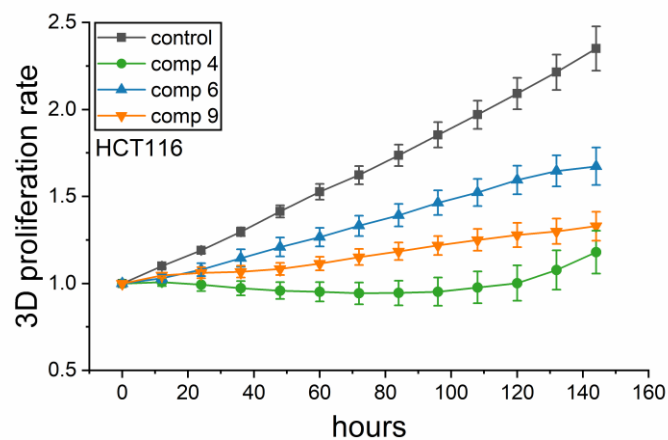
(B) Quantification of IMP2 protein levels of HCT116 and SW480 cells, treated with compound **4** (40  $\mu$ M), **6** (50  $\mu$ M), or **9** (50  $\mu$ M) for 24 h. Data are normalized to tubulin and are represented as means  $\pm$  SEM, n=2.



**Supplementary Figure S14. *In vitro* actions of compounds on 2D tumor cell proliferation**

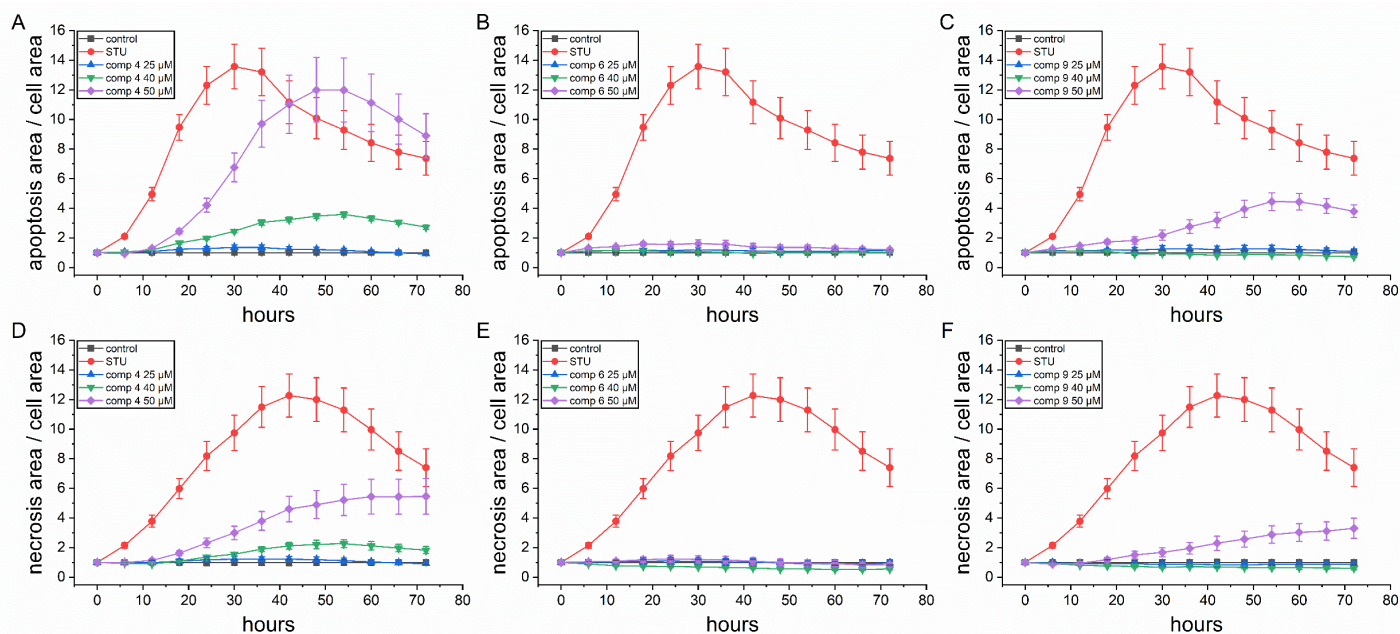
Live-cell microscopy-based analysis of compound-induced anti-proliferative activity. Confluency of (A-C) HCT116 and (D-F) Huh7 cells was monitored in an IncuCyte® S3 system during compound (4, 6, 9) or control treatment over 72 h and normalized to the point of treatment (0 h). Data are represented as means  $\pm$  SEM, n=3 (quadruplicates).





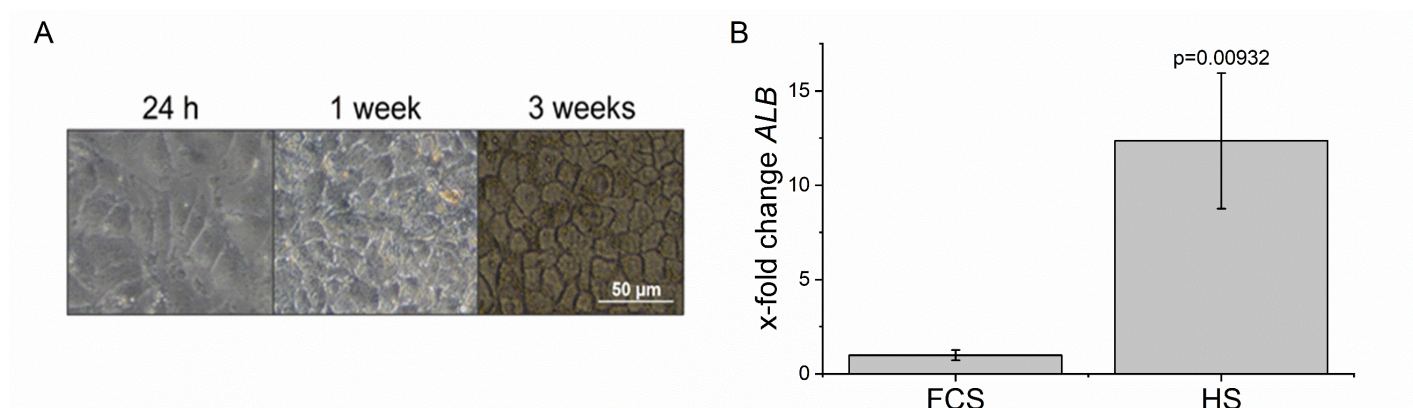
**Supplementary Figure S15. *In vitro* actions of compounds on tumor cell proliferation**

Live-cell microscopy-based analysis of compound-induced anti-proliferative activity. 3-day old HCT116 (left panel) and SW480 (right panel) spheroids were treated with 50  $\mu$ M of the respective compounds and the spheroid area was monitored by the IncuCyte® S3 system. The spheroid area was normalized to the first measuring point after treatment. Data are represented as means  $\pm$  SEM, n=3 (quadruplicates).



**Supplementary Figure S16. Evaluation of compound-induced cell death**

Live cell microscopy-based analysis of cell death upon compound treatment. HCT116 cells were stained for (A–C) caspase 3/7 activity and (D–F) cell membrane permeability and monitored in an IncuCyte® S3 system during compound (4, 6, 9) or vehicle control treatment over 72 h. The apoptosis inducer staurosporine (STU, 1  $\mu$ M) was used as positive control. Fluorescent signals from apoptotic (caspase 3/7 active) and necrotic (permeable membrane) cells were normalized to cell confluency and the time point of treatment (0h). Data are represented as means  $\pm$  SEM, n=3 (quadruplicates).



**Supplementary Figure S17. Differentiation process of Huh7 in human serum**

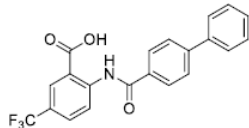
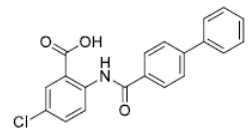
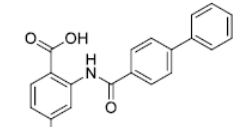
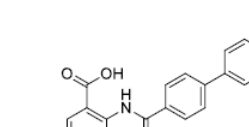
Huh7 cells were differentiated in media supplemented with 2% human serum (HS) for 3 weeks.

(A) Cell morphology was monitored microscopically 24 h, 1 week, and 3 weeks after medium change.

(B) Gene expression of albumin (*ALB*) in differentiated and FCS-cultured cells. RNA was isolated 3 weeks after medium change and gene expression was assessed by qPCR. Values were normalized to the housekeeping gene *RPS11*. Data (x-fold of values for FCS-cultured cells) are represented as means  $\pm$  SEM, n=4 (triplicates).

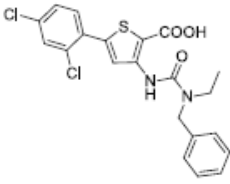
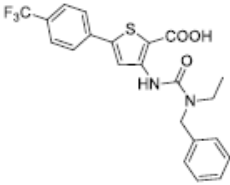
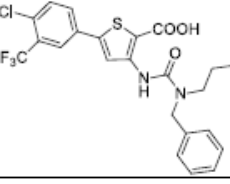
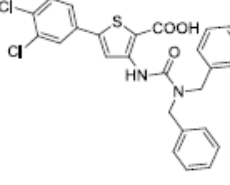
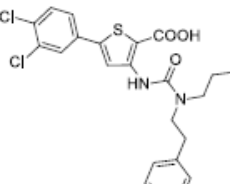
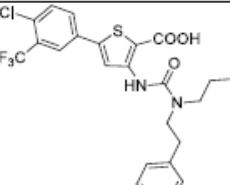
**Supplementary Table 1. Descriptive data of class A compounds**

Class A compounds: Molecular weights, chemical structures, and analytical data. Abbreviations: carbon-NMR ( $^{13}\text{C}$  NMR); coupling constant (J); deuterated dimethyl sulfoxide (DMSO- $d_6$ ); doublet peak (d); liquid chromatography–mass spectrometry (LC/MS); melting point (mp); multiplet peak (m); parts per million (ppm); proton NMR ( $^1\text{H}$  NMR); quartet peak (q); retention time (tr); singlet peak (s); triplet peak (t).

#	Reference	MW	Structure	Analytical Data
1	Hinsberger et al., 2014	385.34		$^1\text{H}$ NMR (500 MHz, DMSO- $d_6$ ) $\delta$ ppm 12.41 (s, 1H) 8.93 (d, $J$ = 8.8 Hz, 1H) 8.28 (d, $J$ = 1.9 Hz, 1H) 8.03 - 8.06 (m, 2H) 8.01 (dd, $J$ = 8.8, 1.9 Hz, 1H) 7.87 - 7.92 (m, 2H) 7.73 - 7.78 (m, 2H) 7.47 - 7.54 (m, 2H) 7.40 - 7.46 (m, 1H). $^{13}\text{C}$ NMR (126 MHz, DMSO- $d_6$ ) $\delta$ ppm 168.90, 164.66, 144.27, 144.01, 138.75, 132.65, 130.85 (q, $J_{\text{CF}}$ = 3.7 Hz) 129.06, 128.35, 127.94 (q, $J_{\text{CF}}$ = 3.7 Hz), 127.84, 127.20, 126.95, 123.80 (q, $J_{\text{CF}}$ = 271.3 Hz), 122.76 (q, $J_{\text{CF}}$ = 33.0 Hz) 120.36, 116.81. LC/MS: $m/z$ = 386, 771; $t_R$ = 14.60 min; 99.76% pure (UV). White solid; mp. 264.8-266.0°C.
2	Hinsberger et al., 2014	351.78		$^1\text{H}$ NMR (500 MHz, DMSO- $d_6$ ) $\delta$ ppm 12.14 (s, 1H) 8.74 (d, $J$ = 9.1 Hz, 1H) 8.02 - 8.05 (m, 2H) 8.00 (d, $J$ = 2.8 Hz, 1H) 7.86 - 7.91 (m, 2H) 7.75 - 7.79 (m, 2H) 7.73 (dd, $J$ = 9.0, 2.7 Hz, 1H) 7.48 - 7.54 (m, 2H) 7.41 - 7.47 (m, 1H). $^{13}\text{C}$ NMR (126 MHz, DMSO- $d_6$ ) $\delta$ ppm 168.77, 164.38, 143.80, 139.88, 138.82, 133.87, 132.92, 130.39, 129.08, 128.32, 127.75, 127.18, 126.96, 126.53, 121.81, 118.55. LC/MS: $m/z$ = 352, 354; $t_R$ = 14.32 min; 99.33% pure (UV). White solid; mp. 273.8-278.9°C.
3	Hinsberger et al., 2014	385.34		$^1\text{H}$ NMR (500 MHz, DMSO- $d_6$ ) $\delta$ ppm 12.35 (s, 1H) 9.10 (d, $J$ = 1.6 Hz, 1H) 8.26 (d, $J$ = 8.2 Hz, 1H) 8.04 - 8.08 (m, 2H) 7.89 - 7.95 (m, 2H) 7.75 - 7.81 (m, 2H) 7.57 (dd, $J$ = 8.2, 1.6 Hz, 1H) 7.49 - 7.55 (m, 2H) 7.41 - 7.47 (m, 1H). $^{13}\text{C}$ NMR (126 MHz, DMSO- $d_6$ ) $\delta$ ppm 169.00, 164.78, 143.98, 141.41, 138.79, 133.38 (q, $J_{\text{CF}}$ = 32.0 Hz), 132.67, 132.45, 129.08, 128.35, 127.80, 127.23, 126.97, 122.88 (q, $J_{\text{CF}}$ = 273.1 Hz), 119.15 (q, $J_{\text{CF}}$ = 3.7 Hz), 116.25 (q, $J_{\text{CF}}$ = 3.7 Hz). LC/MS: $m/z$ = 386, 427, 771; $t_R$ = 14.11 min; 100.00% pure (UV). White solid; mp. 244.9-245.8°C.
4	Hinsberger et al., 2014	401.34		$^1\text{H}$ NMR (500 MHz, DMSO- $d_6$ ) $\delta$ ppm 12.17 (s, 1H) 8.81 (d, $J$ = 9.1 Hz, 1H) 8.03 - 8.06 (m, 2H) 7.92 (dd, $J$ = 3.0, 0.8 Hz, 1H) 7.88 - 7.91 (m, 2H) 7.74 - 7.78 (m, 2H) 7.68 - 7.74 (m, 1H) 7.49 - 7.53 (m, 2H) 7.41 - 7.46 (m, 1H). $^{13}\text{C}$ NMR (126 MHz, DMSO- $d_6$ ) $\delta$ ppm 168.61, 164.48, 143.86, 142.66 (q, $J_{\text{CF}}$ = 1.8 Hz), 140.12, 138.82, 132.88, 129.08, 128.33, 127.80, 127.20, 127.04, 126.96, 123.31, 121.90, 118.55, 120.04 (q, $J_{\text{CF}}$ = 256.0 Hz). LC/MS: $m/z$ = 402, 803; $t_R$ = 14.58 min; 100.00% pure (UV). White solid; mp. 244.6-245.9°C.

**Supplementary Table 2. Descriptive data of class B compounds**

Class B compounds: Molecular weights, chemical structures, and analytical data. Abbreviations: carbon-NMR ( $^{13}\text{C}$  NMR); coupling constant (J); deuterated dimethyl sulfoxide (DMSO- $d_6$ ); doublet peak (d); liquid chromatography–mass spectrometry (LC/MS); melting point (mp); multiplet peak (m); parts per million (ppm); proton NMR ( $^1\text{H}$  NMR); quartet peak (q); retention time ( $t_R$ ); singlet peak (s); triplet peak (t).

#	Reference	MW	Structure	Analytical Data
5	Sahner et al., 2013	449.35		$^1\text{H}$ -NMR (300 MHz, DMSO- $d_6$ ): $\delta$ ppm 1.15 (t, $J = 7.1$ , 3H), 3.39 (q, $J = 7.1$ , 2H), 4.58 (s, 2H), 7.23 – 7.37 (m, 5H), 7.53 (dd, $J = 8.5$ , 2.1, 1H), 7.68 (d, $J = 8.5$ , 1H), 7.79 (d, $J = 2.1$ , 1H), 8.27 (s, 1H), 10.04 (s, 1H), 13.51 (br. s., 1H). $^{13}\text{C}$ NMR (75 MHz, DMSO- $d_6$ ): $\delta$ ppm 13.1, 41.8, 49.3, 108.8, 122.1, 127.1, 128.1, 128.5, 130.1, 130.5, 132.1, 132.4, 134.3, 138.0, 142.3, 145.6, 153.0, 165.6. LC/MS: $m/z = [\text{M}+\text{H}^+]$ 448.55, $[2\text{M}+\text{H}^+]$ 898.57 $t_R = 15.14$ min, 99.3% pure (UV). mp: 212 – 214°C.
6	Sahner et al., 2013	448.46		$^1\text{H}$ -NMR (300 MHz, DMSO- $d_6$ ): $\delta$ ppm 1.16 (t, $J = 7.1$ , 3H), 3.40 (q, $J = 7.1$ , 2H), 4.59 (s, 2H), 7.24 – 7.38 (m, 5H), 7.79 (d, $J = 8.4$ , 2H), 7.91 (d, $J = 8.1$ , 2H), 8.41 (s, 1H), 10.05 (s, 1H), 13.47 (br. s., 1H). $^{13}\text{C}$ NMR (75 MHz, DMSO- $d_6$ ): $\delta$ ppm 13.1, 41.8, 49.3, 108.2, 124.0 (q, $^1J_{\text{CF}} = 272.0$ Hz), 126.2 (q, $^3J_{\text{CF}} = 3.7$ Hz), 126.4, 127.2, 128.4, 128.5, 129.3 (q, $^3J_{\text{CF}} = 32.0$ Hz), 136.5, 138.1, 145.3, 146.7, 153.0, 165.6. LC/MS: $m/z = [\text{M}+\text{H}^+]$ 448.68, $[2\text{M}+\text{H}^+]$ 896.93 $t_R = 14.59$ min, 98.02% pure (UV). mp: 193 – 194°C.
7	Sahner et al., 2013	510.96		$^1\text{H}$ -NMR (300 MHz, DMSO- $d_6$ ): $\delta$ ppm 0.88 (t, $J = 7.5$ , 3H), 1.25 – 1.37 (m, 2H), 1.52 – 1.63 (m, 2H), 3.32 (t, $J = 7.5$ , 2H), 4.59 (s, 2H), 7.23 – 7.38 (m, 5H), 7.77 – 7.80 (s, 1H), 7.98 – 8.00 (m, 2H), 8.38 (s, 1H), 10.08 (s, 1H), 13.56 (br. s., 1H). LC/MS: $m/z = [\text{M}+\text{H}^+]$ 510.85; $t_R = 16.16$ min, 100% pure (UV).
8	Sahner et al., 2013	511.42		$^1\text{H}$ -NMR (300 MHz, DMSO- $d_6$ ): $\delta$ ppm 4.64 (s, 4H), 7.26 – 7.38 (m, 10H), 7.65 – 7.71 (m, 2H), 7.94 (s, 1H), 8.35 (s, 1H), 10.08 (s, 1H), 12.66 (br. s., 1H). $^{13}\text{C}$ NMR (75 MHz, DMSO- $d_6$ ): $\delta$ ppm 49.9, 50.1, 118.8, 128.9, 127.1, 127.3, 127.3, 128.6, 128.6, 128.9, 130.0, 131.4, 131.6, 131.8, 132.1, 133.3, 137.2, 144.2, 146.2, 153.5, 165.4. LC/MS: $m/z = [\text{M}+\text{H}^+]$ 511.35; $t_R = 16.36$ min, 95.70% pure (UV). mp: 190 – 191°C.
9	Sahner et al., 2013	477.40		$^1\text{H}$ -NMR (300 MHz, DMSO- $d_6$ ): $\delta$ ppm 0.88 (t, $J = 7.4$ , 3H), 1.60 (q, $J = 7.4$ , 2H), 2.89 (t, $J = 7.4$ , 2H), 3.25 (t, $J = 7.4$ , 2H), 3.50 (q, $J = 7.4$ , 2H), 7.19 – 7.32 (m, 5H), 7.65 – 7.71 (m, 2H), 7.93 (d, $J = (\text{dd}, J = 1.1, 1\text{H})$ ), 8.33 (s, 1H), 10.03 (s, 1H), 13.56 (br. s., 1H). $^{13}\text{C}$ NMR (75 MHz, DMSO- $d_6$ ): $\delta$ ppm 11.0, 21.2, 34.1, 49.0, 49.1, 197.7, 118.7, 125.9, 126.2, 127.3, 128.4, 128.8, 131.4, 131.6, 132.1, 133.3, 138.7, 144.4, 146.7, 152.6, 165.8. LC/MS: $m/z = [\text{M}+\text{H}^+]$ 476.89, $[2\text{M}+\text{H}^+]$ 954.65 $t_R = 16.58$ min, 98.83% pure (UV). mp: 178 – 179°C.
10	Sahner et al., 2013	524.98		$^1\text{H}$ -NMR (300 MHz, DMSO- $d_6$ ): $\delta$ ppm 0.88 (t, $J = 7.3$ , 3H), 1.25 – 1.37 (m, 2H), 1.50 – 1.60 (m, 2H), 2.89 (t, $J = 7.8$ , 2H), 3.29 (t, $J = 8.1$ , 2H), 3.50 (t, $J = 8.2$ , 2H), 7.18 – 7.37 (m, 5H), 7.78 – 7.81 (m, 1H), 7.99 – 8.01 (m, 2H), 8.38 (s, 1H), 10.04 (s, 1H), 13.61 (br. s., 1H). LC/MS: $m/z = [\text{M}+\text{H}^+]$ 524.86 $t_R = 16.85$ min, 96.95% pure (UV).

**Supplementary Table 3. IC<sub>50</sub> values of hit compounds**

Metabolic activity was determined by MTT assay 96 h after treatment with hit compounds or DMSO solvent control. IC<sub>50</sub> values were calculated using non-linear regression analysis. n=2-5 (triplicates).

<b>IC<sub>50</sub> values [μM]</b>						
	<b>MCF7</b>	<b>HCT116</b>	<b>SW480</b>	<b>HepG2</b>	<b>Huh7</b>	<b>Hep3B</b>
<b>1</b>	43.6	48.1	35.1	30.7	34.7	54.7
<b>2</b>	46.7	29.9	22.5	29.1	40.9	45.5
<b>3</b>	> 80	53.2	78.5	75.0	34.5	58.0
<b>4</b>	48.1	31.0	18.2	29.6	33.3	35.5
<b>5</b>	> 80	62.6	61.2	> 80	> 80	> 80
<b>6</b>	55.1	46.9	49.0	42.9	45.4	52.6
<b>7</b>	> 80	44.7	27.1	35.0	38.8	47.7
<b>8</b>	50.3		37.1	33.6	43.5	
<b>9</b>	70.0	37.8	36.8	35.7	24.9	39.8
<b>10</b>	58.0	37.5	41.4	35.0	44.3	46.2

**Supplementary Table 4. Sequences of siRNA oligonucleotides used in IMP2 knockdown**

Individual sequences of the 4-oligo siRNA mixture purchased from Qiagen to knock down IMP2 and the random RNA oligo sequence.

Oligo RNA	Sequence (5' - 3')
oligo 1	CAGGGCGTTAAATTCACAGAT
oligo 2	TCCGCTAGCCAAGAACCTATA
oligo 3	CAGCGAAAGGATGGTCATCAT
oligo 4	CCCGGGTAGATATCCATAGAA
random	AACACGTCTATACGC